

## Supporting Information

### A Mesoporous Metal-Organic Framework Constructed from a Nanosized $C_3$ -symmetric Linker and $[\text{Cu}_{24}(\text{isophthalate})_{24}]$ Cuboctahedra

Yong Yan,<sup>1</sup> Sihai Yang,<sup>1</sup> Alexander J. Blake,<sup>1</sup> William Lewis,<sup>1</sup> Eric Poirier,<sup>2</sup> Sarah A. Barnett<sup>3</sup>, Neil R. Champness,<sup>1</sup> Martin Schröder<sup>1\*</sup>

1. School of Chemistry, University of Nottingham, University Park, Nottingham NG7 2RD (UK)

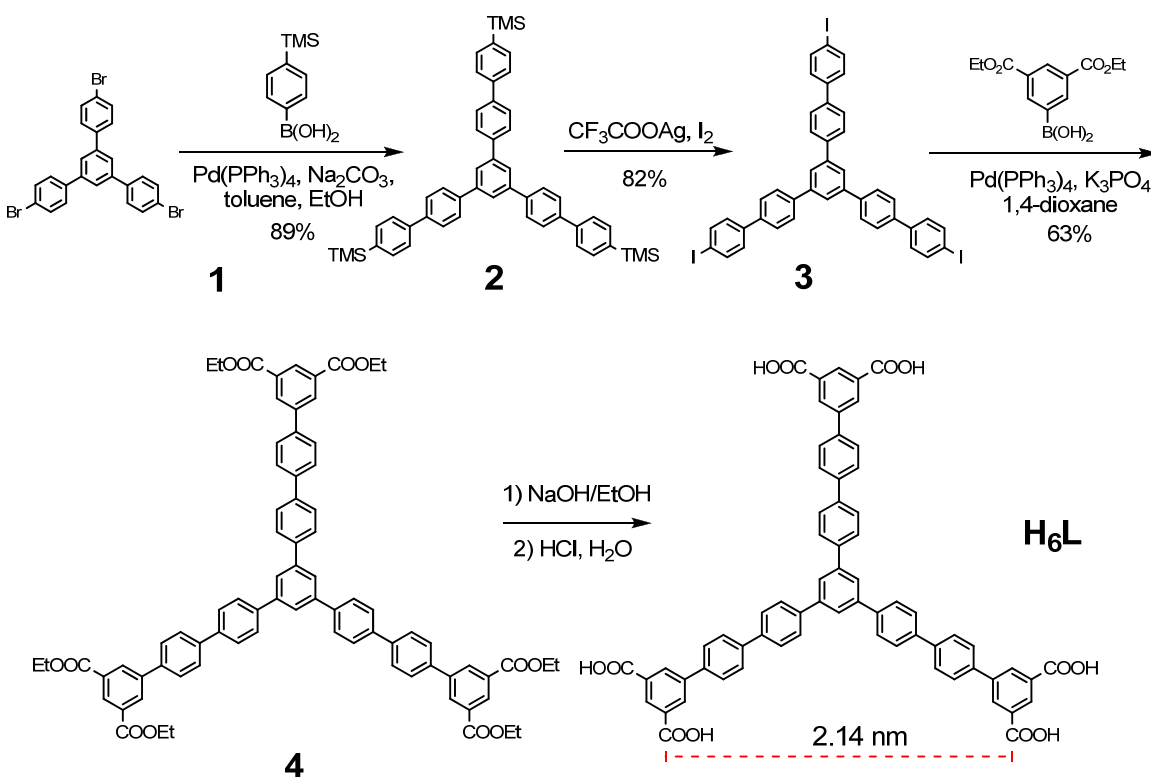
Fax: +44 115 951 3563

E-mail: M.Schroder@nottingham.ac.uk

2. Optimal Inc, Plymouth, Michigan 48170 USA.

3. Diamond Light Source, Diamond House, Harwell Science and Innovation Campus, Didcot, Oxfordshire, OX11 0DE.

### 1. Synthesis of H<sub>6</sub>L



#### Synthesis of **2**.

A mixture of 1,3,5-tri(*p*-bromophenyl)benzene (**1**) (3.9 g, 7.2 mmol), 4-(trimethylsilyl)phenylboronic acid (5.0 g, 25.8 mmol), aqueous  $\text{Na}_2\text{CO}_3$  (2M, 30 mL), toluene (100 mL) and EtOH (30 mL) was degassed under Ar for 30 min before  $[\text{Pd}(\text{PPh}_3)_4]$  (0.49 g, 0.43 mmol) was added. The mixture was heated to reflux under Ar overnight. After the mixture was cooled to room temperature, volatile solvents were removed under reduced pressure, and the residue extracted into  $\text{CHCl}_3$  and washed with water and brine, and dried over  $\text{MgSO}_4$ . The  $\text{CHCl}_3$  was removed on a rotary evaporator, and the crude product purified by column chromatography (silica gel) using hexane/ $\text{CH}_2\text{Cl}_2$  (2:1, v/v) as eluent to yield compound **2** (4.8 g, 89 %).  $^1\text{H}$  NMR (300 MHz,  $\text{CDCl}_3$ ):  $\delta$  7.913 (s, 3 H), 7.836 (d,  $J$  = 8.4 Hz, 6 H), 7.762 (d,  $J$  = 8.4 Hz, 6 H), 7.679 (m, 12 H), 0.346 (s, 27 H).

### Synthesis of 3.

To a mixture of compound **2** (3.0 g, 4.0 mmol), silver trifluoroacetate (3.2 g, 14.4 mmol) and CHCl<sub>3</sub> (80 mL) which had been refluxed at 70 °C for 15 min, was slowly added a solution of I<sub>2</sub> (3.7 g, 14.4 mmol) in THF (20 mL). The mixture was refluxed for another 4 h and cooled to room temperature before being poured into a large quantity of water and then extracted with CHCl<sub>3</sub> (3 × 300 mL). The combined organic layer was dried over anhydrous Na<sub>2</sub>SO<sub>4</sub> and the solvent removed under reduced pressure. The crude product was purified by recrystallisation from hot CHCl<sub>3</sub> to afford pure **3** as a white solid (3.0 g, 82 %). <sup>1</sup>H NMR (300 MHz, CDCl<sub>3</sub>): δ 7.888 (s, 3 H), 7.837 (d, *J* = 1.8 Hz, 6 H), 7.809 (d, *J* = 1.8 Hz, 6 H), 7.711 (d, *J* = 8.4 Hz, 6 H), 7.429 (d, *J* = 8.4 Hz, 6 H); <sup>13</sup>C NMR (300 MHz, CDCl<sub>3</sub>): δ 141.91, 140.36, 140.09, 139.38, 137.97, 128.90, 127.87, 127.39, 125.11, 93.25.

### Synthesis of 4.

Compound **3** (2.0 g, 2.2 mmol), diethylisophthalate-5-boronic acid (2.1 g, 7.9 mmol), and K<sub>3</sub>PO<sub>4</sub> (4.5 g, 21.2 mmol) were mixed with 1,4-dioxane (100 mL), and the mixture de-aerated under Ar for 20 min. [Pd(PPh<sub>3</sub>)<sub>4</sub>] (152 mg, 0.13 mmol) was added to the stirred reaction mixture under Ar, and the mixture heated at 90 °C for 48 h under a constant flow of Ar, after which 1,4-dioxane was removed under vacuum. The resultant solid was treated with a mixture of water (100 mL) and CHCl<sub>3</sub> (100 mL). The organic layer was washed with NH<sub>4</sub>Cl solution (3 × 50 mL), brine and then dried over MgSO<sub>4</sub>. The solvent was removed under reduced pressure and the residue was purified by column chromatography using ethyl acetate/hexane (1:3) as eluent to yield pure **4** (1.65 g, 63 % yield). <sup>1</sup>H NMR (CDCl<sub>3</sub>, 300 MHz): δ = 8.702 (t, *J* = 1.5 Hz, 3 H), 8.552 (d, *J* = 1.5 Hz, 6 H), 7.953 (s, 3 H), 7.901 – 7.826 (m, 24 H), 4.489 (q, 12 H), 1.481 (t, 18 H); <sup>13</sup>C NMR (CDCl<sub>3</sub>, 300 MHz): δ = 165.867, 142.003, 141.332, 140.464, 140.327, 139.703, 138.241, 132.088, 131.601, 129.362, 127.9, 127.718, 127.687, 127.596, 125.129, 61.532, 14.428.

### Synthesis of H<sub>6</sub>L<sup>3</sup>.

Compound **4** (1.5 g, 1.6 mmol) was suspended in a mixture of THF (50 mL) and EtOH (50 mL), to which was added 2 M KOH aqueous solution (50 mL). The mixture was stirred under reflux overnight. The volatile solvents (THF and EtOH) were removed under reduced pressure. Dilute HCl was added to the remaining aqueous solution until the solution was at pH = 3. The precipitate was collected by filtration, washed with water and EtOH, and dried to give H<sub>6</sub>L<sup>3</sup> (1.1 g, 96% yield). <sup>1</sup>H NMR (DMSO-*d*<sub>6</sub>, 300 MHz): δ 8.489 (t, *J* = 1.5 Hz, 3 H),

8.450 (d,  $J = 1.5$  Hz, 6 H), 8.048 – 8.021 (m, 9 H), 7.931 – 7.855 (m, 18 H);  $^{13}\text{C}$  NMR (DMSO- $d_6$ , 300 MHz):  $\delta$  167.100, 141.637, 140.921, 139.886, 139.840, 139.109, 138.028, 132.896, 131.494, 129.256, 128.327, 128.007, 127.885, 127.641, 124.885. MS (ESI) m/z (%) = [M–3H] $^{3-}$  341.0839 (100%); [M–2H] $^{2-}$  512.1316 (92%); [M–H] $^-$  1025.2528 (19%).

## 2. Preparation of NOTT-119, $[\text{Cu}_3(\text{C}_{66}\text{H}_{36}\text{O}_{12})(\text{H}_2\text{O})_3] \cdot 35\text{DMF} \cdot 35\text{H}_2\text{O}$ .

$\text{H}_6\text{L}$  (0.1 g, 0.1 mmol) and  $\text{Cu}(\text{NO}_3)_2 \cdot 3\text{H}_2\text{O}$  (0.22 g, 0.9 mmol) were mixed and dispersed in DMF/ $\text{H}_2\text{O}$  (15 mL, 5:1 v/v). HCl (2 M, 0.3 mL) was added to the mixture which was mixed thoroughly. The solution was heated without stirring in an 85 °C oil bath for 18 h, and a large amount of microcrystalline product precipitated. The blue crystalline product was separated by filtration and washed with warm DMF, and dried briefly in air. Yield: 0.12 g (28%). Anal. Calcd (Found) for  $\text{C}_{171}\text{H}_{357}\text{Cu}_3\text{N}_{35}\text{O}_{85}$ : C, 46.11 (47.05); H, 8.08 (7.12); N, 11.01 (10.16)%.

## 3. Single Crystal X-ray Structure Determination on NOTT-119

**Crystal Data:**  $\text{C}_{171}\text{H}_{357}\text{Cu}_3\text{N}_{35}\text{O}_{85}$ ,  $M = 4454.54$ ,  $T = 120$  (2) K,  $\lambda = 0.6889$  Å, cubic, space group  $Fm\bar{3}m$ ,  $a = 56.296(7)$  Å,  $V = 178416(36)$  Å $^3$ ,  $Z = 32$ ,  $D_x = 1.327$  g cm $^{-3}$ ,  $\mu = 0.380$  mm $^{-1}$ ,  $F(000) = 76640$ , crystal size  $0.05 \times 0.05 \times 0.05$  mm, 45135 reflections collected, 2377 unique ( $R_{\text{int}} = 0.141$ ), multi-scan absorption correction, refinement by full-matrix least-squares on  $F^2$ , data / restraints / parameters = 2377 / 109/ 146, GOF on  $F^2 = 1.53$ , final  $R_1$  [ $I > 2\sigma(I)$ ] = 0.131,  $wR_2$  (all data) = 0.391, difference Fourier extrema  $\pm 0.42$  eÅ $^{-3}$ . Despite the use of synchrotron radiation, no significant diffraction was observed beyond  $\theta = 16^\circ$ .

Single crystal diffraction data were collected on Beamline I19 of Diamond Light Source. Details of the data collection are included in the CIF. The structure was solved by direct methods and developed by difference Fourier techniques, both using the SHELXTL software package.<sup>1</sup> The hydrogen atoms of the ligands were placed geometrically and refined using a riding model; the hydrogen atoms of the coordinated water molecules could not be located but are included in the formula. The unit cell volume includes a large region of disordered solvent which could not be modelled as discrete atomic sites: we therefore employed PLATON/SQUEEZE<sup>2</sup> to calculate the contribution of the solvent region to the diffraction and thereby produced a set of solvent-free diffraction intensities. Due to the small size of the available crystals (ca. 0.000125 mm $^3$ ) and the large fractional pore volume (ca. 80%), and despite our use of a dedicated beamline for chemical crystallography on a third-generation

synchrotron radiation source, the intensity, quality and extent of the diffraction data available were all very poor. This is reflected in low resolution, high discrepancy indices and limited precision. We believe that there is inherent diffraction limit beyond which no diffraction is recorded, so we excluded data above this limit. Nevertheless, the principal structural features of NOTT-119 are clearly seen in the final structure. The final formula was calculated from the crystallographic data combined with elemental analysis data.

**Table S1.** Crystal data and structure refinement details for **NOTT-119**.

NOTT-119	
Formula	C <sub>171</sub> H <sub>357</sub> Cu <sub>3</sub> N <sub>35</sub> O <sub>85</sub>
Formula weight	4454.54
Temperature	120 (2) K
Radiation type	Synchrotron
λ (Å)	0.6889
Crystal System	Cubic
Space Group	<i>Fm-3m</i>
Unit Cell Dimensions	<i>a</i> = 56.296(7) Å
Volume	178416(36) Å <sup>3</sup>
Z	32
Density	1.327 g cm <sup>-3</sup>
Absorption coefficient	0.380 mm <sup>-1</sup>
<i>F</i> (000)	76640
Crystal Size	0.05 × 0.05 × 0.05 mm <sup>3</sup>
Reflections collected	45135
Independent reflections	2377 [ <i>R</i> <sub>int</sub> = 0.141]
Absorption correction	multi-scan
Refinement method	Full-matrix least-squares on <i>F</i> <sup>2</sup>
Data / restraints / parameters	2377 / 109/ 146
GOF on <i>F</i> <sup>2</sup>	1.53
Final <i>R</i> indices [ <i>I</i> > 2 σ( <i>I</i> )]	<i>R</i> <sub>1</sub> = 0.131, <i>wR</i> <sub>2</sub> = 0.372
Final <i>R</i> indices (all data)	<i>R</i> <sub>1</sub> = 0.150, <i>wR</i> <sub>2</sub> = 0.391
Difference Fourier map: maximum peak, minimum trough ( <i>e</i> Å <sup>-3</sup> )	0.42, -0.42

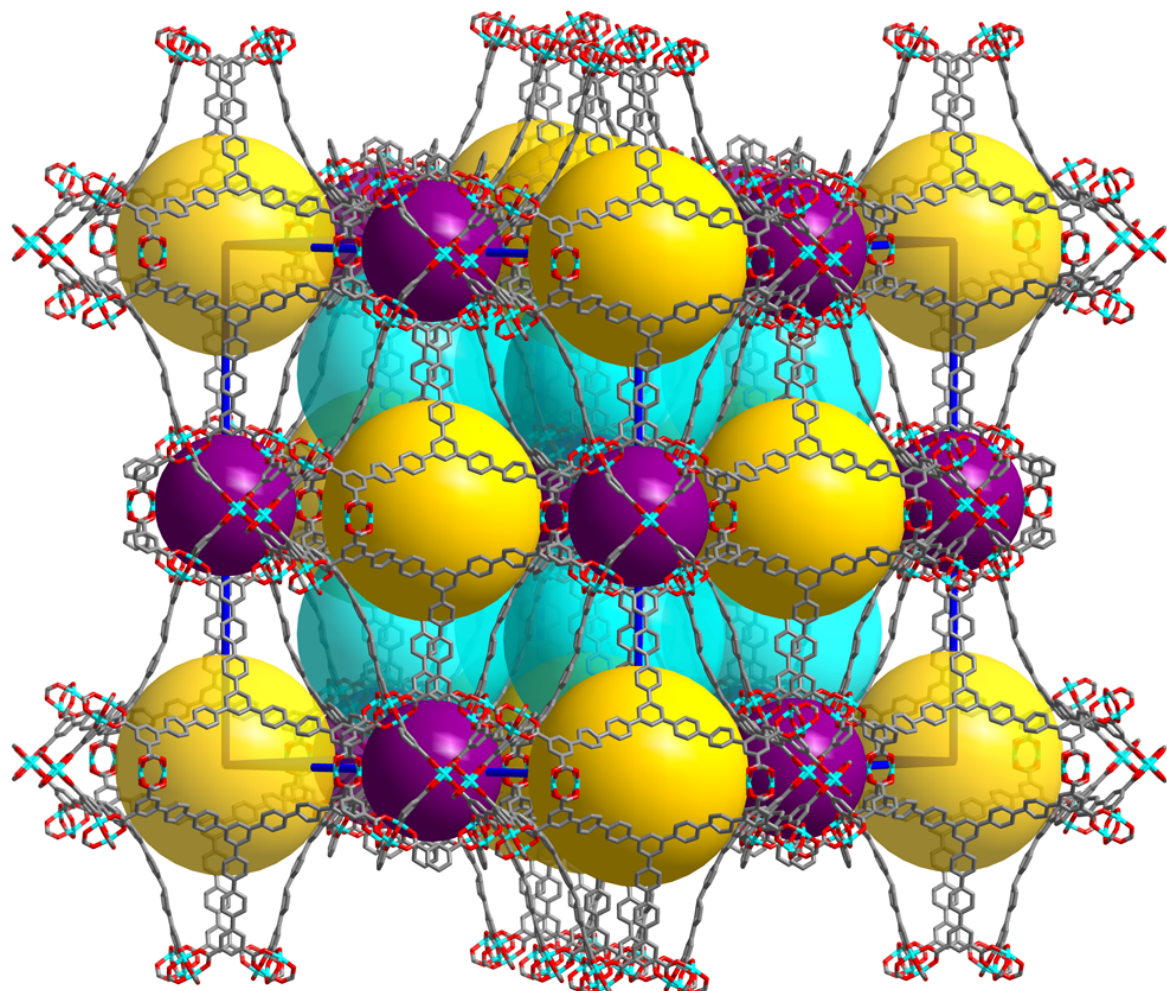


**Figure S1.** View of the packing of the three types of cages in the structure of NOTT-119.

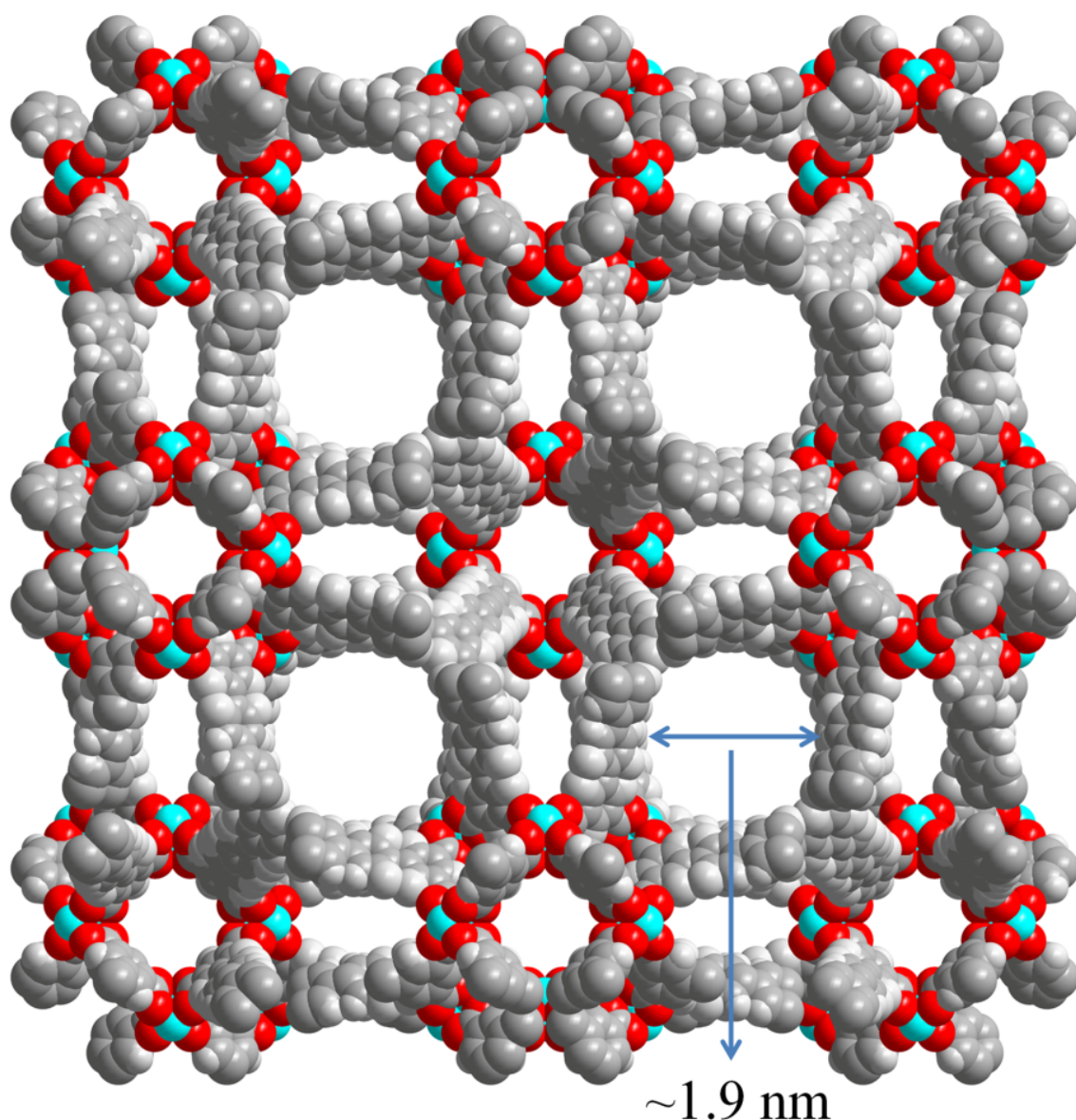


**Figure S2.** Space filling representation of **NOTT-119** viewed along the  $a$  axis in the crystal lattice.

#### 4. TGA plot

Thermal gravimetric analyse (TGA) was performed under N<sub>2</sub> flow (60 ml/min) with a heating rate of 2 °C/min using a TA SDT-600 thermogravimetric analyzer.

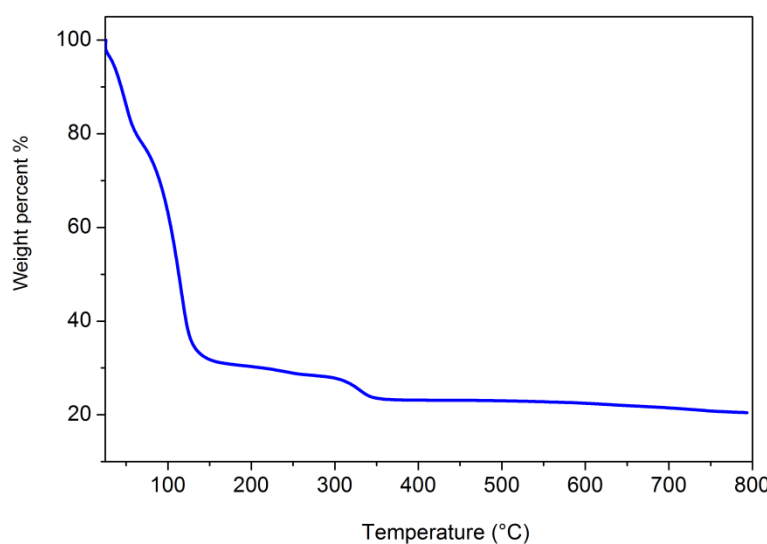


**Figure S3.** TGA plot for as-synthesised NOTT-119.

#### 5. Powder X-ray diffraction (PXRD)

The PXRD pattern of activated NOTT-119a was recorded on a Bruker D8 Advance powder diffractometer with a Cu  $K\alpha$  X-ray source ( $\lambda = 1.54058 \text{ \AA}$ ) operating at 40 kV and 40 mA and a Sol-X detector.

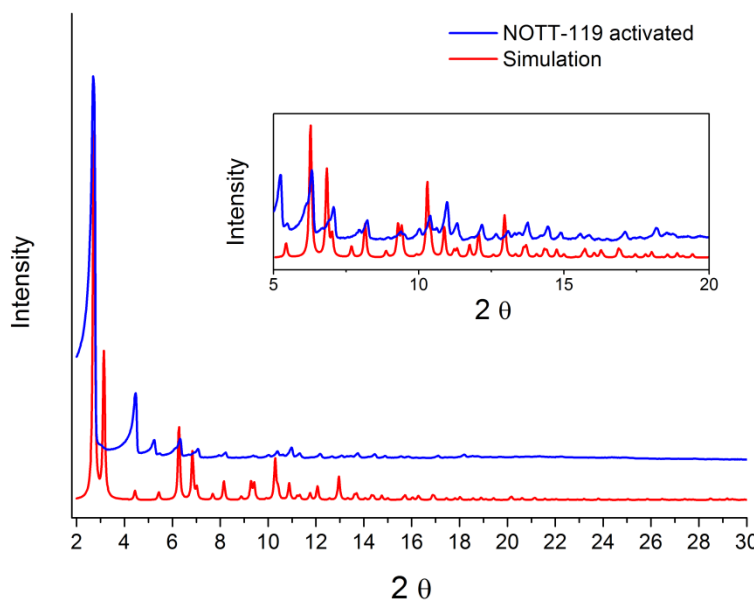


**Figure S4.** PXRD patterns for NOTT-119a. The blue line corresponds to the activated sample obtained by heating the acetone-exchanged sample at 110 °C for 16 h under vacuum.

## 6. Variable temperature PXRD experiments

Variable temperature PXRD experiments were performed on as-synthesised NOTT-119 using synchrotron radiation ( $\lambda = 0.825582 \text{ \AA}$ ). The as-synthesised sample was heated under vacuum and the PXRD patterns were collected at various temperatures (RT, 100, 150 and 200 °C). This study reveals that the as-synthesised NOTT-119 has good thermal stability.

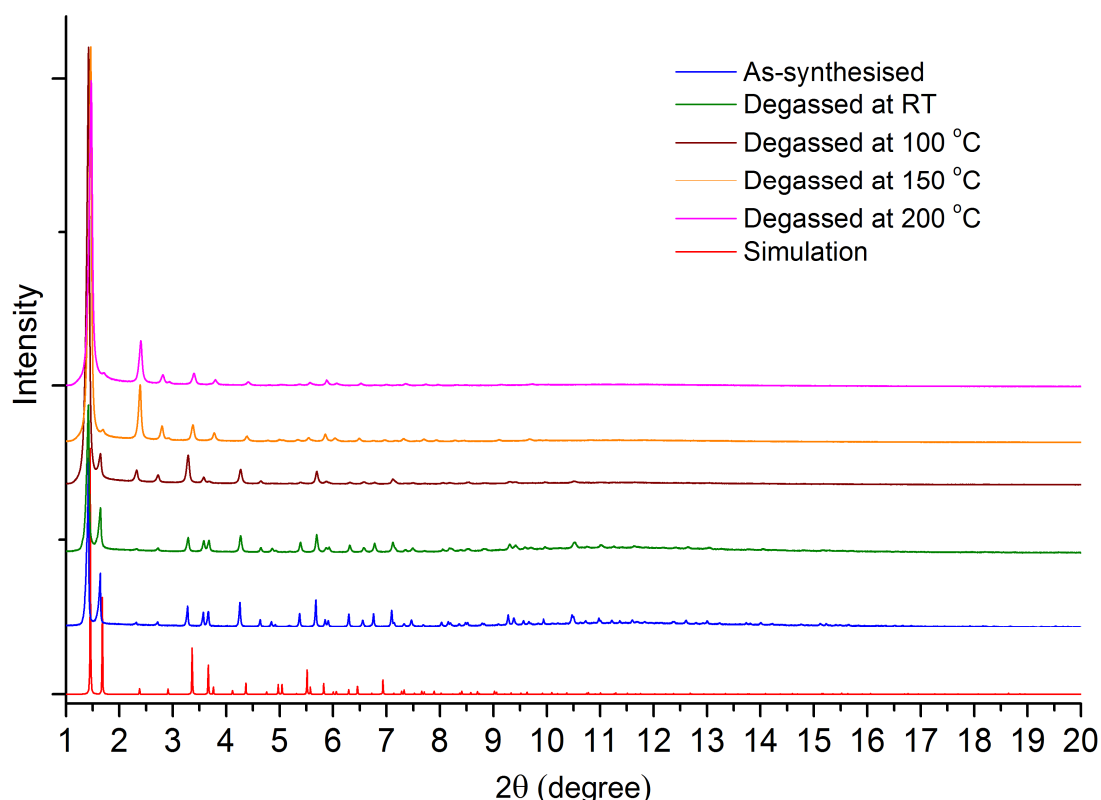


**Figure S5.** PXRD patterns for NOTT-119. The simulated pattern was calculated based upon the single crystal structure.

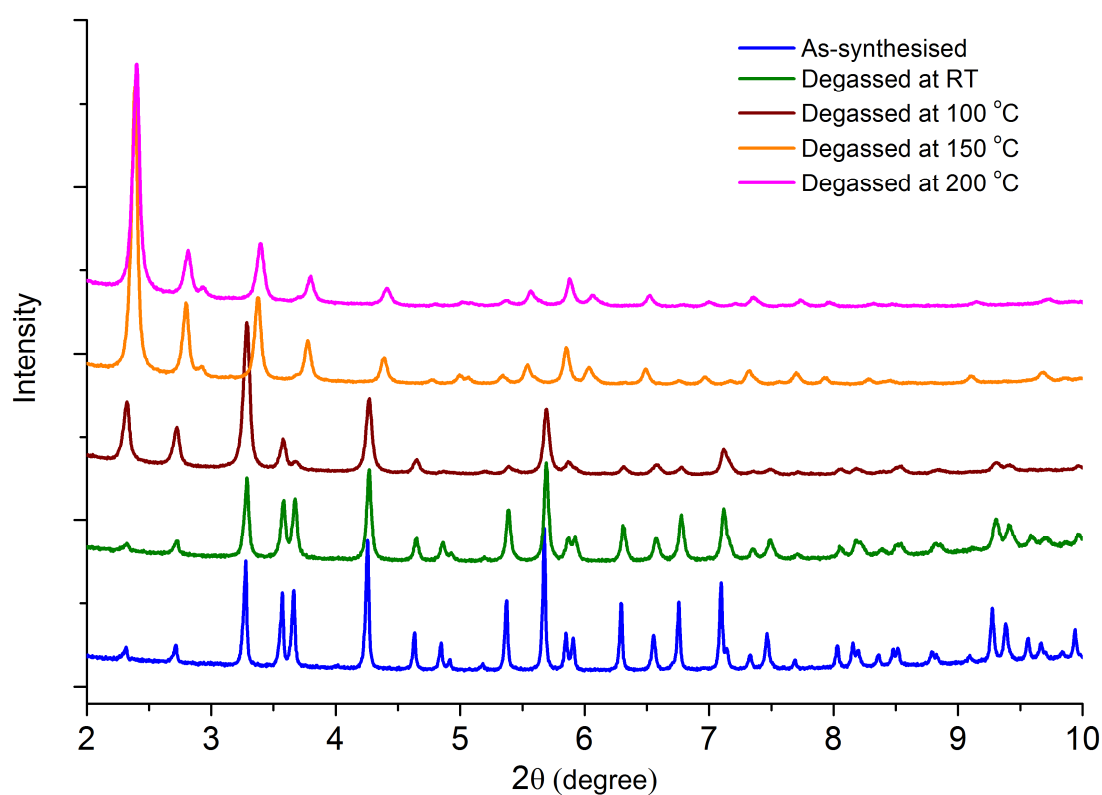


**Figure S6.** PXRD patterns for NOTT-119 in  $2\theta$  range 2–10°.

**Table S2.** Summary of indexing and Le Bail refinement results (using the software TOPAS 4 from Bruker AXS) for the variable-temperature PXRD data for NOTT-119.

Sample	Space group	$a$ (Å)	$V$ (Å $^3$ )	Cell change (%)	$R_{wp}$ (%)
As-synthesised	Fm-3m	57.8040(8)	193141(8)	100	8.73
Degassed at RT	Fm-3m	57.6307(14)	191409(14)	99.10	7.06
Degassed at 100 °C	Fm-3m	57.6219(16)	191321(16)	99.06	6.72
Degassed at 150 °C	Fm-3m	56.0520(16)	176106(16)	91.18	6.66
Degassed at 200 °C	Fm-3m	55.7160(27)	172958(25)	89.55	7.35

The fitting graphs of the PXRD data are shown below (blue: calculated; red: observed; grey: difference):

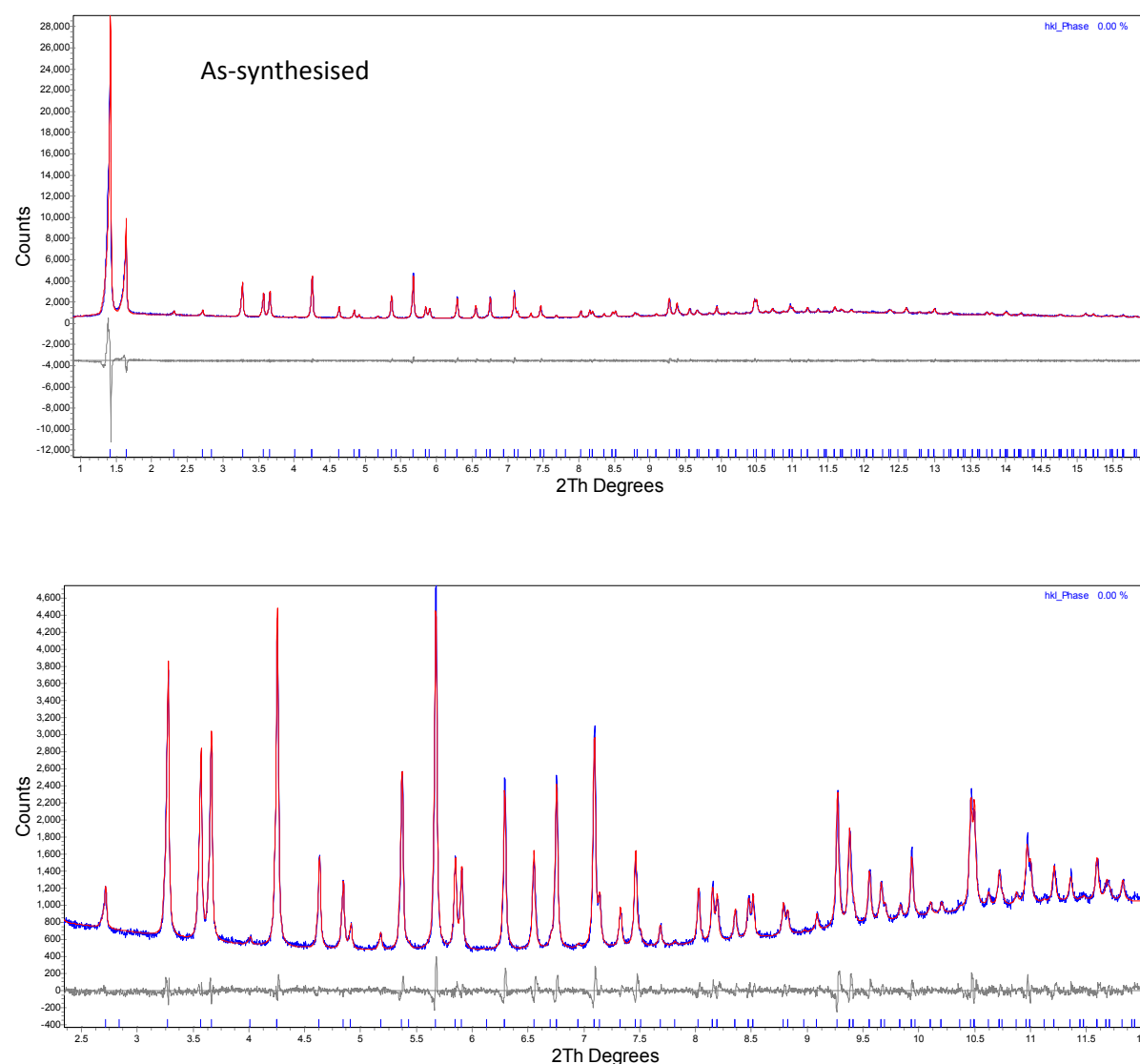


**Figure S7.** Le Bail fitting results for the PXRD pattern of as-synthesised NOTT-119 (top); The high angle region has been magnified for clarity of the plot (bottom).

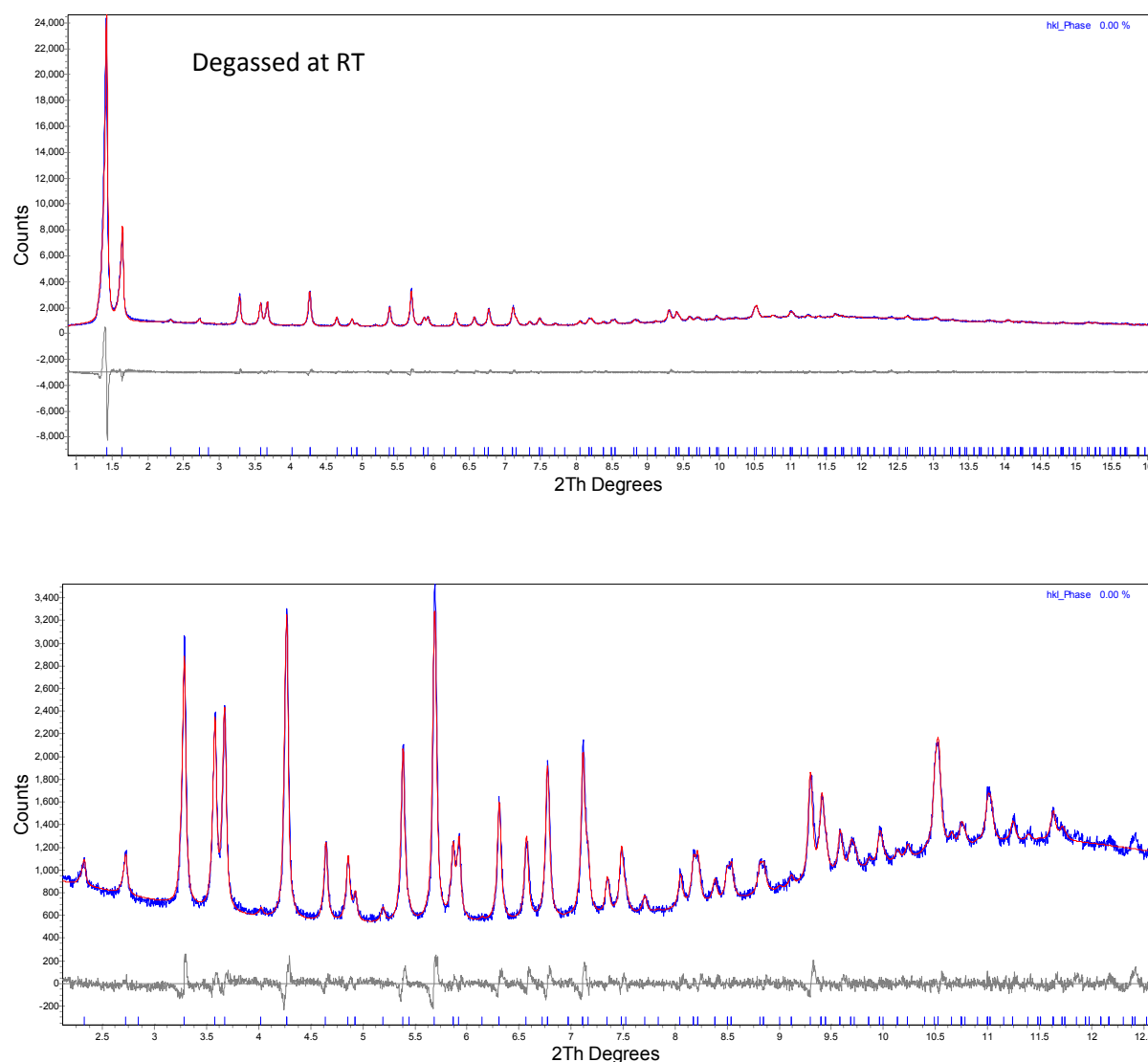


**Figure S8.** Le Bail fitting results for the PXRD pattern of NOTT-119 (degassed at RT); The high angle region has been magnified for clarity of the plot (bottom).

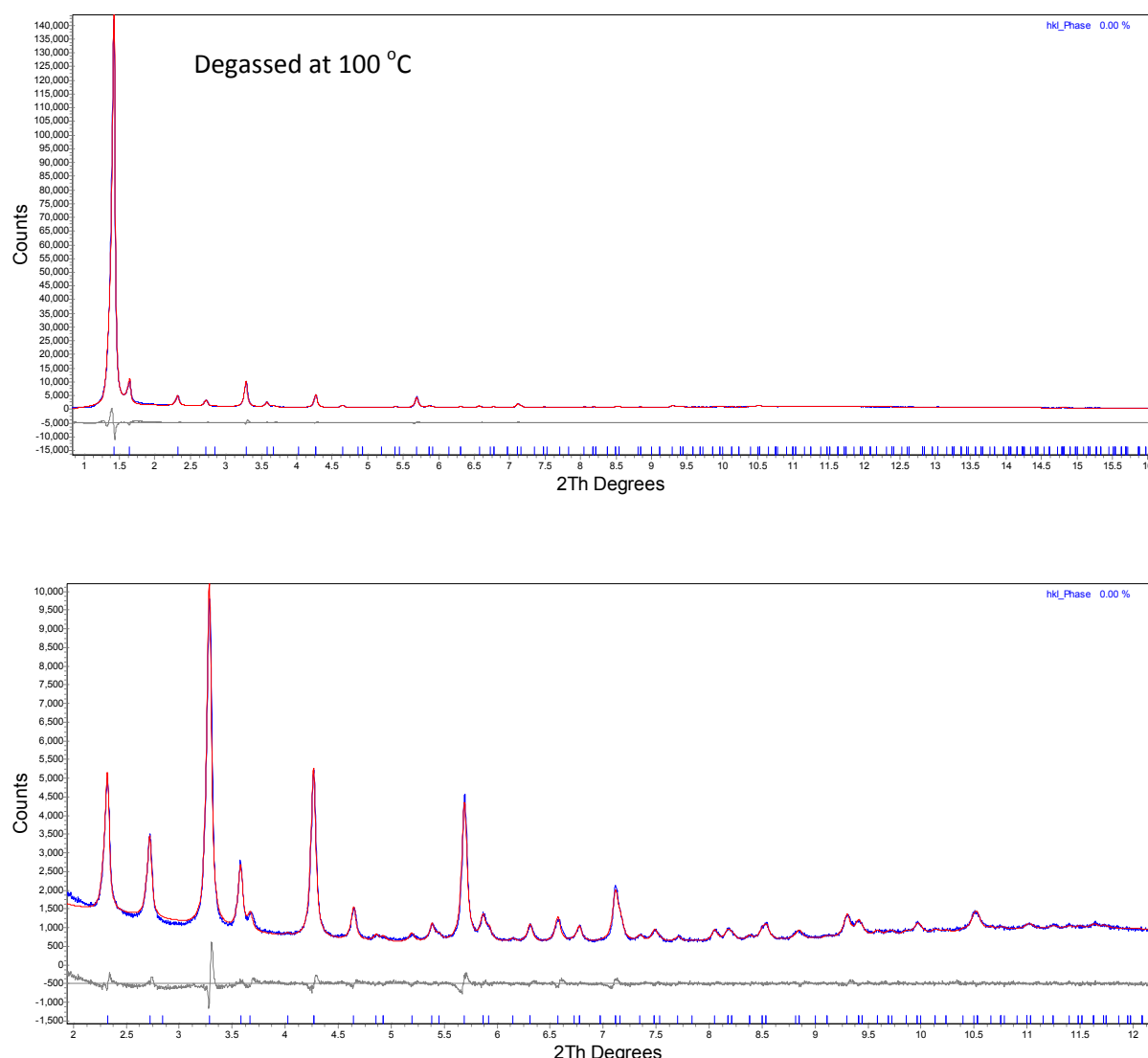


**Figure S9.** Le Bail fitting results for the PXRD pattern of NOTT-119 (degassed at 100 °C); The high angle region has been magnified for clarity of the plot (bottom).

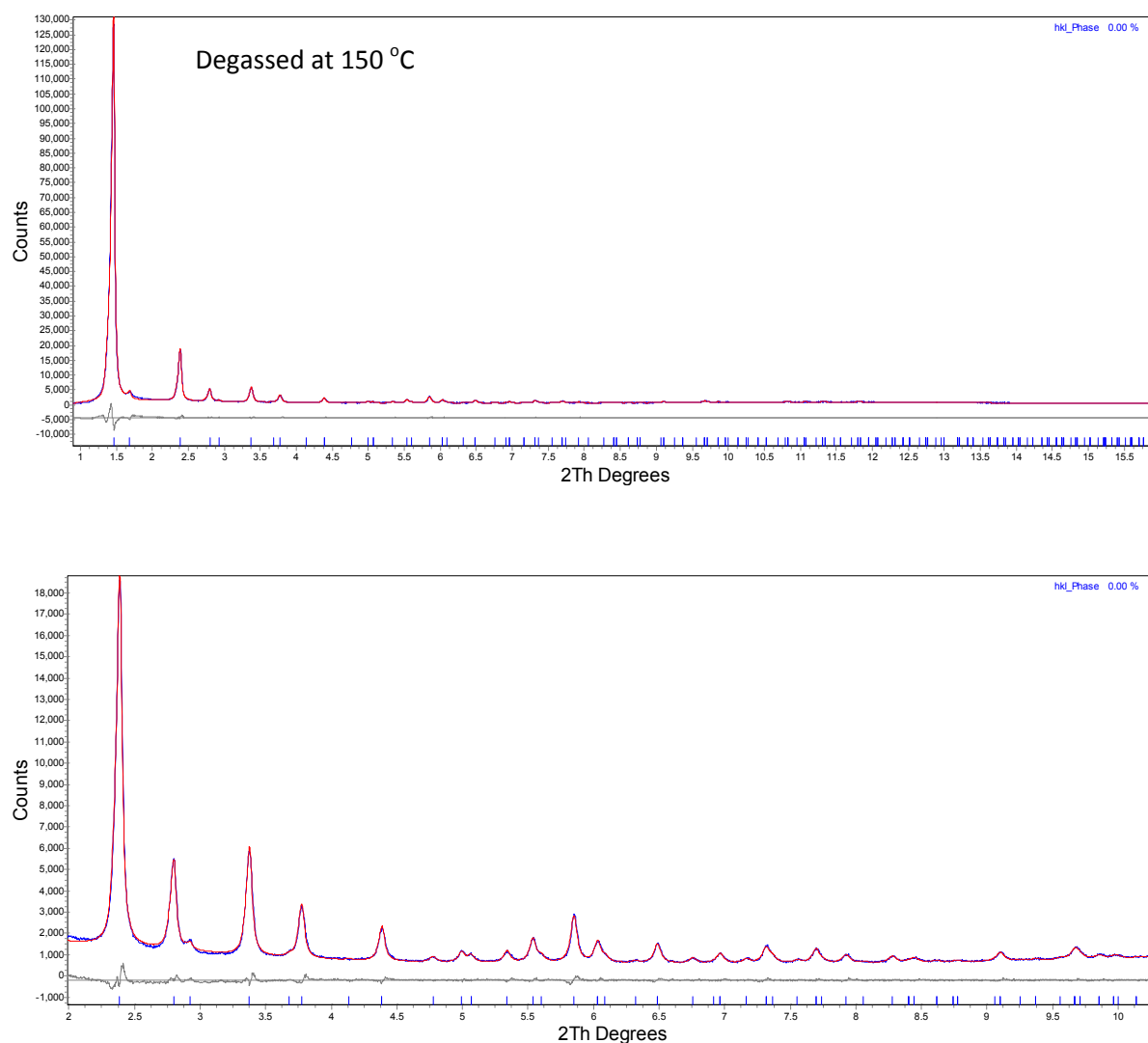


**Figure S10.** Le Bail fitting results for the PXRD pattern of NOTT-119 (degassed at 150 °C); The high angle region has been magnified for clarity of the plot (bottom).

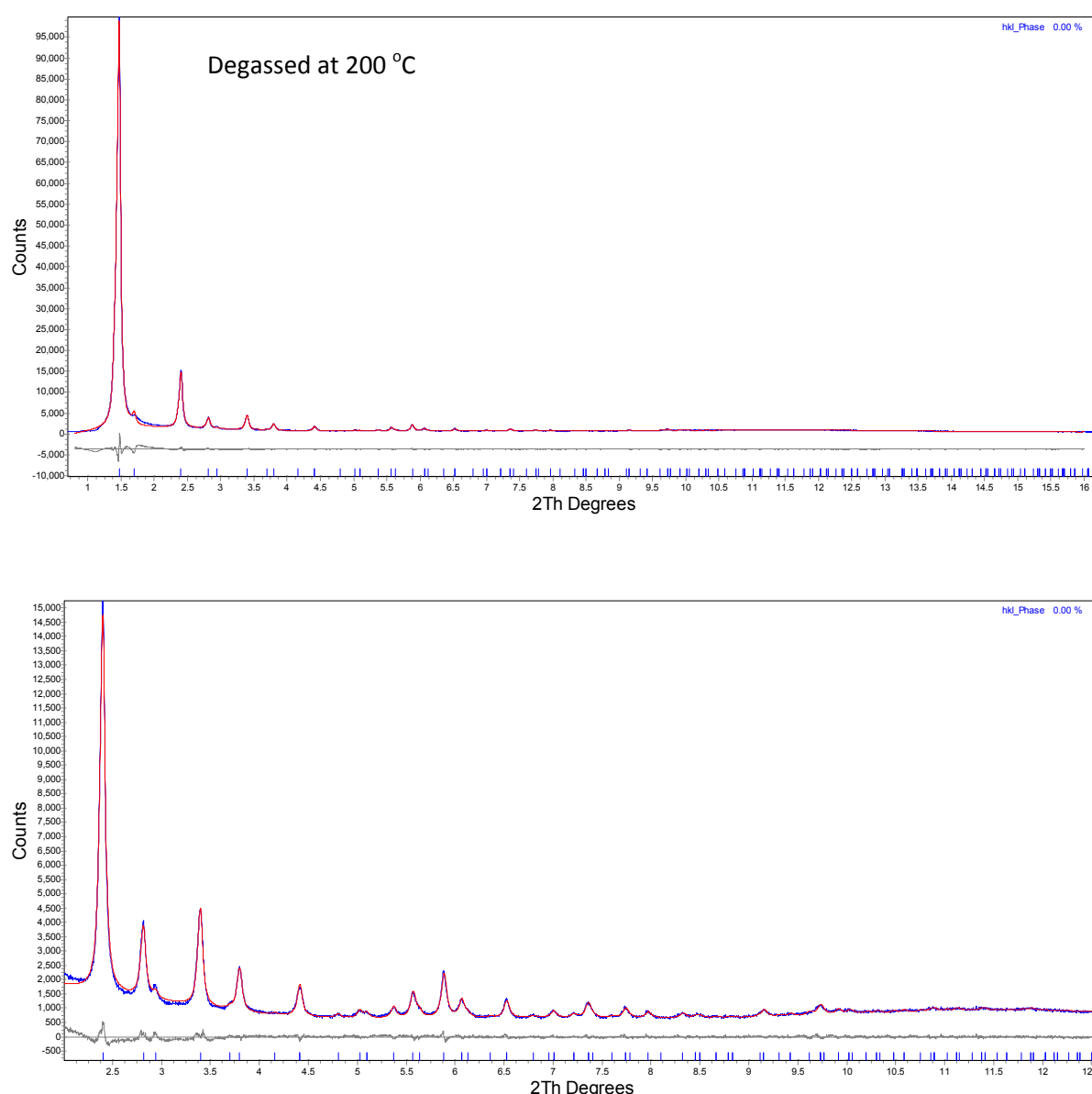


**Figure S11.** Le Bail fitting results for the PXRD pattern of NOTT-119 (degassed at 200 °C); The high angle region has been magnified for clarity of the plot (bottom).

## 7. Low-pressure N<sub>2</sub>, Ar and H<sub>2</sub> adsorption measurements

Low-pressure (< 1 bar) adsorption measurements were performed using an Autosorb 1-MP instrument from Quantachrome Instruments. Ultra-high purity grade N<sub>2</sub>, Ar, He and H<sub>2</sub> were used for adsorption measurements.

**BET plot:**

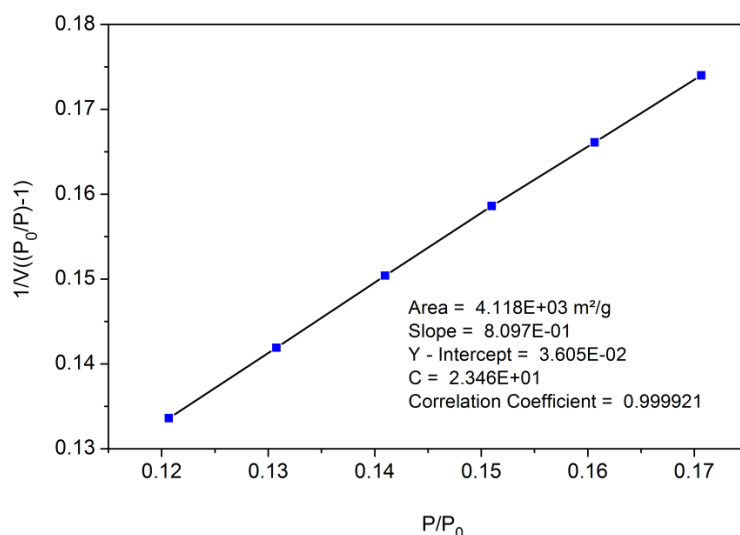


**Figure S12.** Plot of the linear region for the BET analysis. The BET surface area of NOTT-119a was calculated to be 4118 ( $\pm 200$ ) m<sup>2</sup> g<sup>-1</sup> (with a 5% standard uncertainty).

**Pore size distribution**

The pore-size distribution was calculated from analysis of the Ar isotherm (adsorption branch) at 87 K using non-local density functional theory (NLDFT)<sup>3</sup> implementing a hybrid kernel based on a zeolite–silica model containing spherical/cylindrical pores.

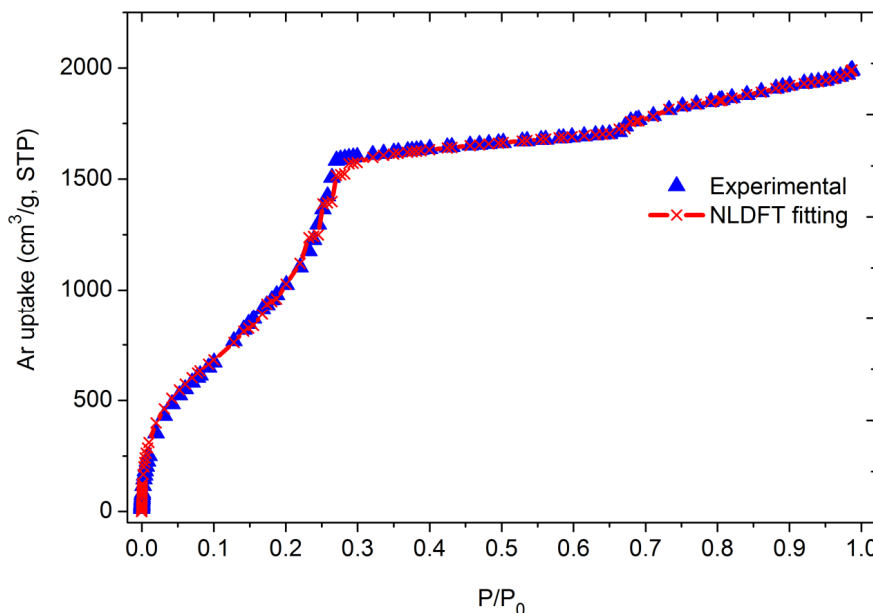


**Figure S13.** Comparison of the NLDFT fitting for the Ar adsorption isotherm with the experimental data.

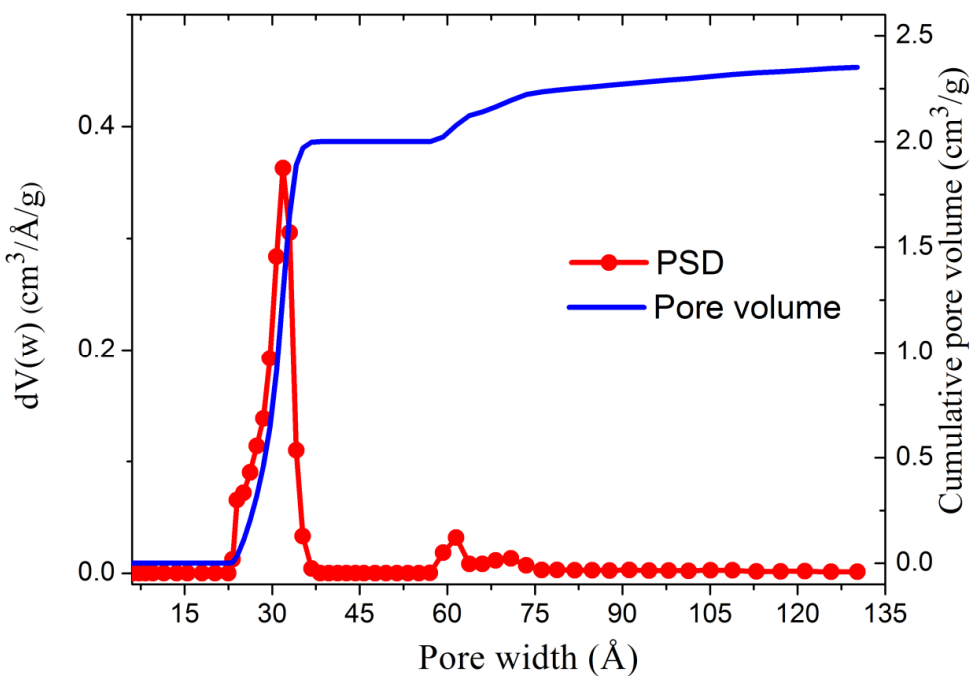


**Figure S14.** Pore size distribution (PSD) plot for NOTT-119 as calculated from experimental Ar adsorption isotherm using NLDFT and the cumulative pore volume from PSD.

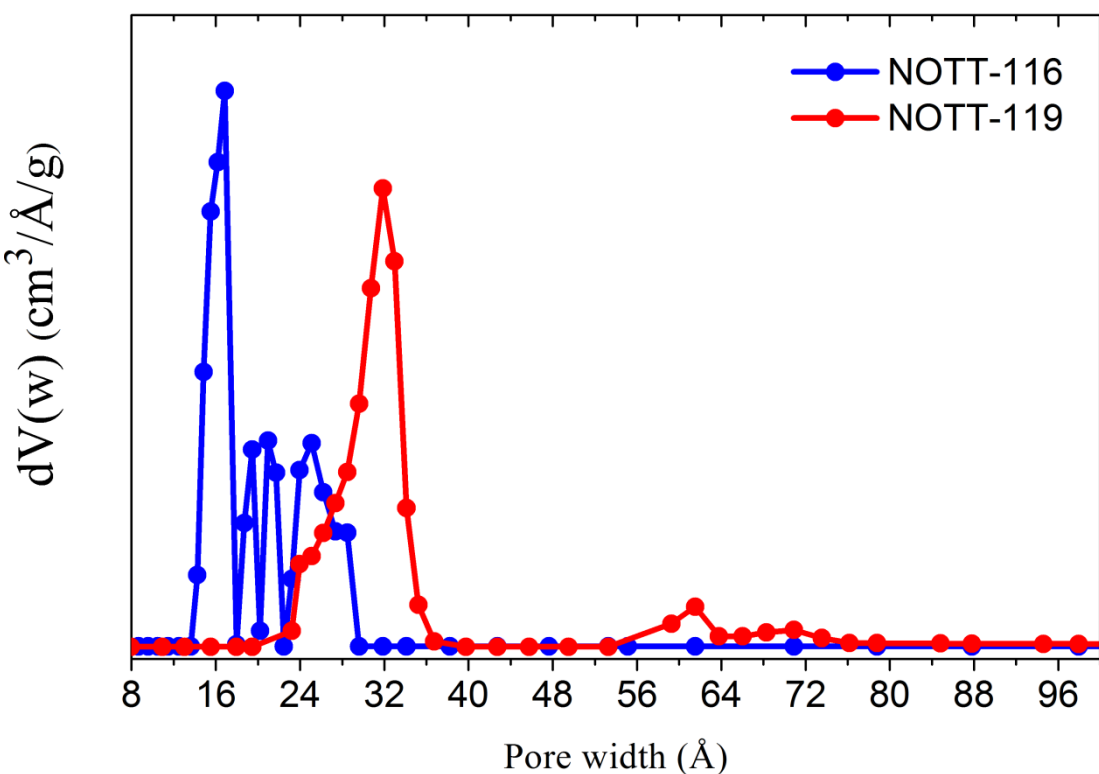


**Figure S15.** Comparison of the pore size distribution plots between NOTT-116<sup>4</sup> and NOTT-119.

**Derivation of the Isosteric Heats of H<sub>2</sub> Adsorption.** A virial-type expression<sup>5</sup> was used to fit the combined isotherm data for NOTT-119a at 78 and 88 K:

$$\ln(P) = \ln(N) + (1/T) \sum_{i=0}^m a_i N^i + \sum_{j=0}^n b_j N^j \quad (1)$$

The values of the virial coefficients  $a_0$  through  $a_m$  were then used to calculate the isosteric heat of adsorption using the following equation:

$$Q_{st} = -R \sum_{i=0}^m a_i N^i \quad (2)$$

Here,  $Q_{st}$  is the coverage-dependent isosteric heat of adsorption and  $R$  is the universal gas constant.

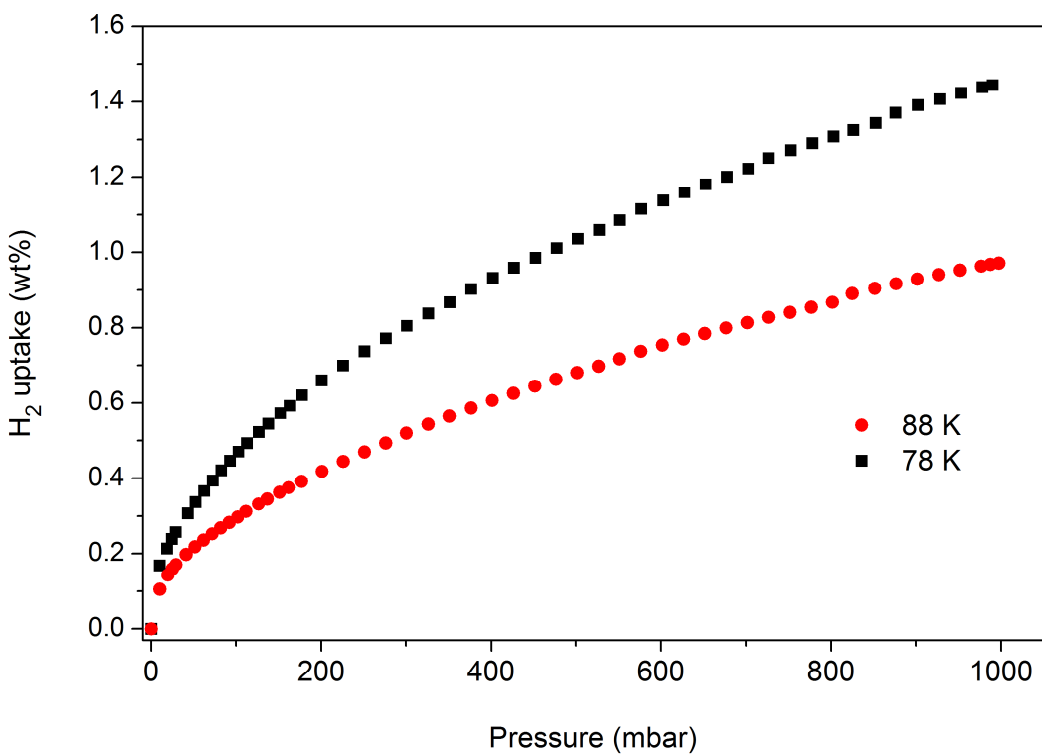


**Figure S16.** H<sub>2</sub> isotherms for NOTT-119a at 78 and 88 K, respectively.

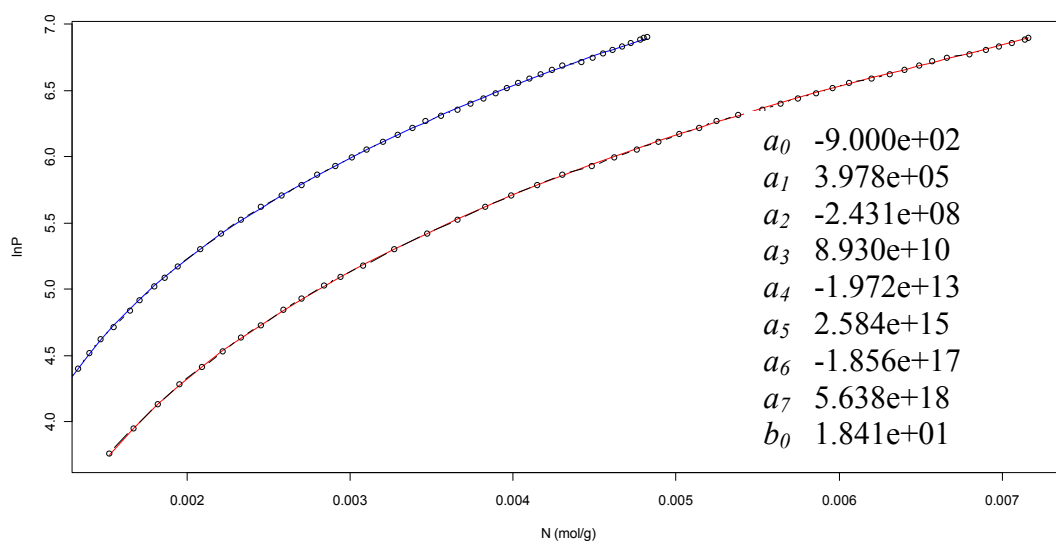


**Figure S17.** Virial analysis of the  $\text{H}_2$  adsorption data for NOTT-119a (red line: 78 K; blue line: 88 K).

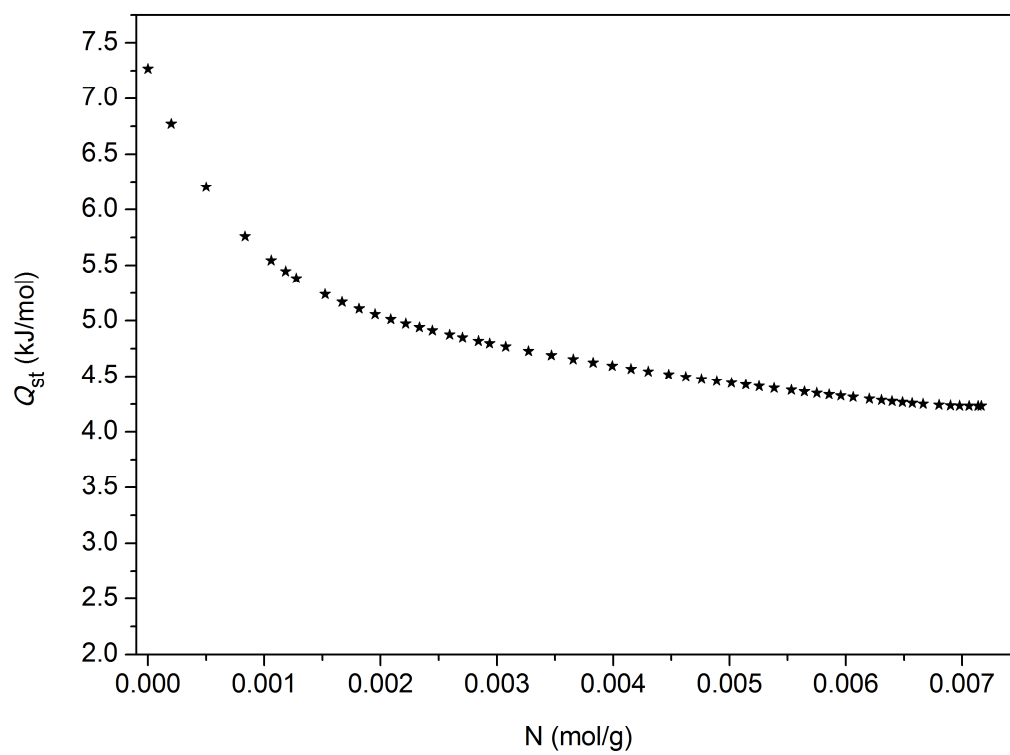


**Figure S18.** Heats of  $\text{H}_2$  adsorption for NOTT-119a.

## 8. High pressure H<sub>2</sub> and CH<sub>4</sub> sorption measurements

Volumetric H<sub>2</sub> and CH<sub>4</sub> sorption measurements were performed at General Motors USA over the pressure range 0–80 bar using an automatically controlled Sievert's apparatus (PCT-Pro 2000 from Hy-Energy LLC).

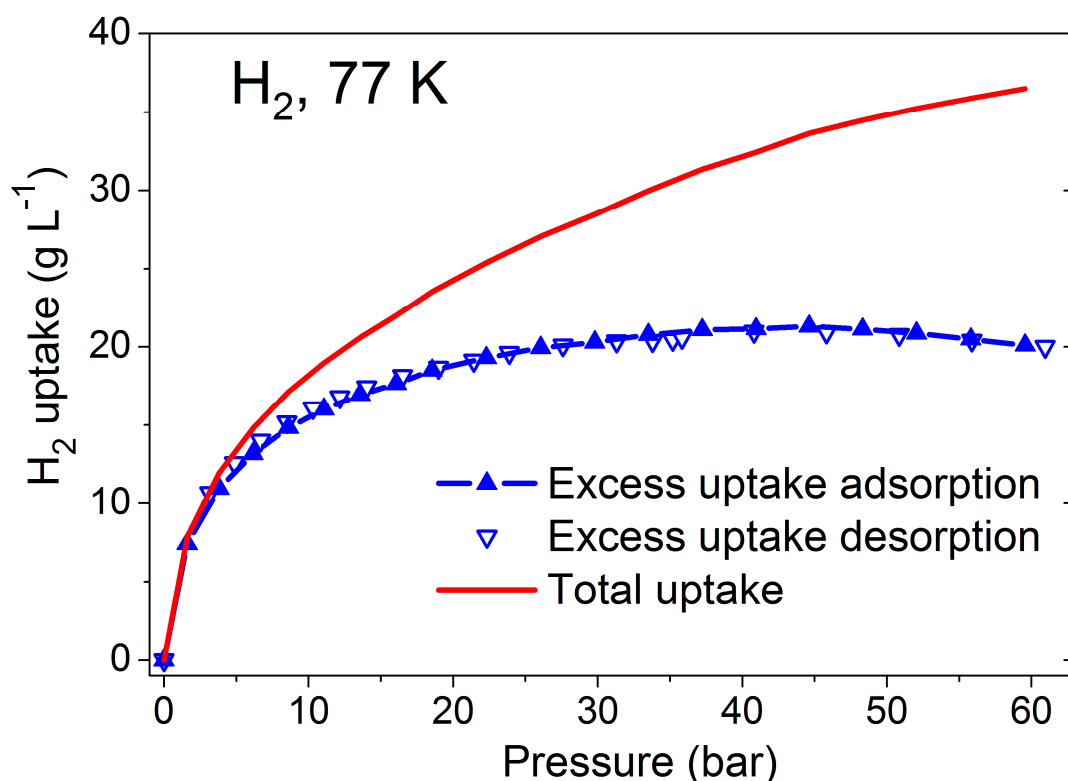


**Figure S19.** Volumetric H<sub>2</sub> sorption isotherms for NOTT-119a.

## References:

1. G. M. Sheldrick, *SHELXS97. Acta Crystallogr., Sect. A* 2008, **64**, 112–122.
2. A. L. Spek, *Acta Crystallogr., Sect. D*, 2009, **65**, 148–155.
3. P. I. Ravikovitch, D. Wei, W. T. Chueh, G. L. Haller and A. V. Neimark, *J. Phys. Chem. B*, 1997, **101**, 3671–3679.
4. Y. Yan, I. Telepeni, S. Yang, X. Lin, W. Kockelmann, A. Dailly, A. J. Blake, W. Lewis, G. S. Walker, D. R. Allan, S. A. Barnett, N. R. Champness and M. Schröder, *J. Am. Chem. Soc.* 2010, **132**, 4092–4094.
5. L. Czepirski and J. Jagiełło, *Chem. Eng. Sci.* 1989, **44**, 797–801.